

Star Formation in Satellite Galaxies¹

C. M. Gutiérrez

Instituto de Astrofísica de Canarias, E-38205 La Laguna, Tenerife, Spain

`cgc@iac.es`

M. S. Alonso²

Consejo Nacional de Investigación Científicas y Técnicas, Argentina

`salonso@casleo.gov.ar`

J. G. Funes, SJ

Vatican Observatory, Univ. of Arizona, Tucson, AZ 85721, USA

and

M. B. Ribeiro

Instituto de Física, Universidade Federal do Rio de Janeiro, Brazil

ABSTRACT

We present narrow-band observations of the H α emission in a sample of 31 satellite orbiting isolated giant spiral galaxies. The sample studied spans the range $-19 < M_B < -15$ mag. The H α emission was detected in all the spiral and irregular objects with fluxes in the range $1.15 - 49.80 \times 10^{-14}$ erg cm $^{-2}$ s $^{-1}$. The average and maximum values for the current star formation rates are 0.68 and 3.66 M $_{\odot}$ yr $^{-1}$ respectively. Maps of the spatial distribution of ionized gas are presented. The star-forming regions show a rich structure in which frequently discrete complexes are imposed over more diffuse structures. In general, the current star formation rates are smaller than the mean values in the past obtained from the current stellar content; this probably indicates a declining rhythm with time in the generation of new stars. However, the reserve of gas is enough to continue fueling the current levels of star formation activity for at least another Hubble time. Four of the objects (NGC 2718b, NGC 4541e, NGC 5965a $_1$ and NGC 5965a $_2$) with higher current star formation rates show clear signs of interaction with close companions of comparable brightness at projected distances of 25, 20 and 2 kpc respectively. The only two galaxies in our sample that do not show star formation activity are members of these interacting systems, and it is unclear if this is a consequence of intrinsic properties (both are Hubble early types) or if it is related with possible disruption of the external parts due to the interaction. In the case of the pair NGC 2718a-b there are indications of gas transport between both galaxies.

Subject headings: galaxies: fundamental parameters – galaxies: photometry – galaxies: structure – galaxies: star formation rate

¹Based on observations with the VATT: the Alice P. Lennon Telescope and the Thomas J. Bannan Astrophysics

Facility.

²Marie Curie Fellowship, Instituto de Astrofísica de Ca-

1. Introduction

Cold dark matter cosmologies predict a hierarchical scenario (e.g., White & Rees 1978) in which small structures are formed first, and then by several processes of merging, accretion, etc., larger structures are generated. Currently, one of the most discussed questions in this field is the so-called “missing satellite problem”; in fact semi-analytic models (Kauffmann et al. 1993) and numerical simulations (Klypin et al. 1999; Moore et al. 1999) of small structure formation in cold dark matter cosmologies predict a number of satellites in the halos of large galaxies an order of magnitude larger than the observed counts in the Local Group. A possible observational incompleteness of factor up to three of the known population of dwarfs orbiting the Milky Way, as has been evaluated by Willman et al. (2004), is not enough to solve the discrepancy. It has also been proposed that star formation in low-mass structures could be inhibited by a strong photo-ionizing background (Somerville 2002), especially at low redshift (Dijkstra et al. 2004).

Reconstructing the evolutionary history of satellites in galactic halos are, then, essential for validating the main predictions of these models. This requires study of the role of physical processes such as interactions, mass losses, morphological transformation and star formation. Obviously, the best studied are the Milky Way and Andromeda halos, although extending the study to other host galaxies is necessary for studying possible variations from halo to halo, which probably depends on the host mass, the merging history, and the environment. That was our motivation to start an observational program that comprises photometry in optical broad- and narrow-band filters for a sample of satellites orbiting external giant spiral galaxies. In previous articles (Gutiérrez et al. 2002; Gutiérrez & Azzaro 2004) we have analyzed the morphology and photometry of about 60 such objects. This analysis enabled us to validate and extend the relations found in the satellites of the Local Group. In this article, we use narrow-band observations in $H\alpha$ to estimate the current star formation rate of a subsample comprising most of the late type objects. We analyze the evolution of star-forming activity with time, and the

relation with morphological type, HI mass, and environment. The paper is organized as follows. Section 2 presents the observations and data reduction; Section 3 and Appendix A present the images and analyze qualitatively the $H\alpha$ maps of each object; the star formation rate estimates are presented in Section 4; the relation between interactions and star formation, and the cosmological evolution of star formation activity are discussed in Sections 5 and 6; finally Section 7 presents the conclusions.

2. Observing program

2.1. The Sample

The initial sample is the catalogue of satellite galaxies compiled by Zaritsky et al. (1997). The catalogue contains 115 objects orbiting 69 primary isolated spiral galaxies. Basically, the satellites were selected according to their relative brightness (at least 2.2 magnitudes fainter than their parents), projected distances (< 500 kpc) and relative velocity (< 500 km s⁻¹) from the primaries. The objects analyzed here correspond to a subsample comprising most of the objects classified by Gutiérrez & Azzaro (2004) as spirals or irregulars. In total, 31 objects have been observed and analyzed (most of the late type objects observable from the northern hemisphere). The objects span a large range in luminosity ($-19 < M_B < -15$), and constitute a sample useful for statistical studies of the population of late-type galaxies present in the halos of large spiral galaxies.

2.2. Observations and data reduction

The $H\alpha$ images and the broad-band for continuum estimation were acquired during three observing runs seven nights each in December 2001, May 2002, and December 2002 with the 1.8 m Vatican Advanced Technology Telescope (VATT) at the Mt Graham International Observatory. Most of the observations analyzed here were obtained in the first two runs and in photometric conditions (for only for two of the galaxies was it possible to make an absolute direct calibration, see next section). A back-illuminated 2048×2048 Loral CCD was used as the detector at the aplanatic Gregorian focus, $f/9$. It yielded a field of view of $6.4' \times 6.4'$ with an image scale of 0.4 pixel⁻¹ after 2×2 pixel binning. The seeing varied be-

tween 1.1" and 2.3" with a mean value of 1.5". For each galaxy we have obtained typically 3×1800 s narrow-band images using an appropriate interference filters with $\sim 70 \text{ \AA}$ widths that isolate the spectral region characterized by the redshifted $H\alpha$ and $[\text{N II}] \lambda 6548, 6583 \text{ \AA}$ emission lines. To cover the range in velocity spanned for the galaxies presented in this work, three filters were needed with central wavelength of 6584.7, 6632.8 and 6736.2 \AA (another filter exists centered at 6683.1 \AA was not necessary for any of the galaxies analyzed in this work). The nominal normalized spectral response of these filters are presented in Figure 1. Table 1 presents a summary of the observations and properties of the images obtained. Each filter is denoted according to its central wavelength in nm.

For absolute astronomical calibration we observed spectrophotometric standard stars from the list provided by Oke (1990). In general, we observed one of these stars just before or after the narrow-band observations for each galaxy. In each case, stars were selected with similar airmass rather than to calibrate the target. The exposure times for these stars range between 12 and 300 s, depending obviously on the magnitude of the star. These details are shown in Table 1. The data were reduced using IRAF packages³. We performed standard data reduction, comprising, bias subtraction, flat-field correction using sky twilight observations in the appropriate filters, alignment of R and narrow-band images, and co-addition of the narrow-band images. This combination eliminates most of the artifacts due to bad pixels or cosmic rays.

To isolate the possible $H\alpha$ emission of the targeted galaxies, the contribution of the stellar continuum emission of the galaxy needs to be removed. This was done by appropriately scaling the R -band image and subtracting it from the $H\alpha$ images. The scaling factor was estimated by comparing the brightness of several field stars in the broad and in the narrow bands respectively. We measured the flux of these stars in a circular aperture ~ 6 FWHM of the image. Depending on the field, the number of stars considered was in the

³IRAF is the Image Reduction and Analysis Facility, written and supported by the IRAF programming group at the National Optical Astronomy Observatory (NOAO) in Tucson, Arizona.

range 3–12, with a typical number of 5.

3. Images of the satellite galaxies

The R -band and $H\alpha$ images, after continuum subtraction, are presented in Figures 2, 3 and 4. We have detected $H\alpha$ emission in all but two galaxies. For most of the galaxies, the $H\alpha$ emission shows a complex morphology in which it is possible to discern diffuse and discrete structures. A description of these images is presented in Appendix A. The identification of interacting systems is based on spatial proximity and on the presence of features in the R band, such as a bridge in the case of the pair NGC 2718a-b, tidal streams in the pair NGC 4541b-e, and distortion of the outer isophotes in the case of the two components of NGC 5965a. For the other galaxies there is also some evidence of current or past interactions on the basis of the proximity to the parent (NGC 3154a), possible companions with unknown redshift (NGC 3735a, NGC 4030b, NGC 4541a and NGC 6181a), knots differentiated from the main body of the galaxy having strong star formation activity (NGC 1961b, NGC 5899a and NGC 7678a), or the presence of possible tidal galaxies (as in NGC 2775c).

4. $H\alpha$ luminosities and star formation rates

We use the SExtractor software (Bertin & Arnouts 1996) to carry out the photometry of the galaxies in the broad and narrow-band filters. We consider two possible estimates for the total flux of the galaxies. The first is the integrated flux in a predefined aperture (the same as for the narrow and broad filter) and the second the flux in the automatic aperture computed in SExtractor according to the extrapolation proposed by Kron (1980). In general, we note that the first method gives more robust values for those galaxies that are more irregular, while the second is more appropriate for objects with a well defined regular profile. In the cases in which a fixed aperture was chosen, we checked that the estimated fluxes are similar to those computed with the subroutine PHOT of IRAF. For the absolute calibration and estimation of $H\alpha$ emission, we follow the procedure detailed in Gil de Paz et al. (2003). Because of the width of our narrow filters, the emission in-

cludes also the contribution of [NII] for which an accurate subtraction would require spectroscopic observations.

One of the objects (NGC 4030b) was observed at two epochs (Dec 2001 and May 2002). We think that the $\sim 10\%$ difference between the estimates of H α fluxes in both observations (1.33 and 1.46×10^{-14} erg cm $^{-2}$ s $^{-1}$ for the observations of December and May respectively) are representative of the statistical uncertainty of our procedure. Another test was to observe the apparently non-interacting early-type galaxy NGC 1620b for which we do not in principle expect significant levels of star-forming activity. For this galaxy we estimate an H α flux after continuum subtraction of -0.87×10^{-14} erg cm $^{-2}$ s $^{-1}$, which in absolute value is well below any of the detections of H α emission. We think that this negative value is not entirely due to the uncertainties in the estimate, but indicates H α in absorption, as is commonly found in early-type galaxies (Kennicutt 1992).

The H α equivalent widths (EWs) represent the ratio between the H α emission and the continuum averaged over the full galaxy. Figure 5 shows the relation between the relative flux of the H α emission and the morphological type. The mean values and 1σ dispersions in H α EWs are 16.4 ± 5.1 , 24.3 ± 9.6 , 18.9 ± 7.7 , and for types 2 (Irr), 3 (Sb/Sc), and 4 (Sa) respectively. The mean values found for the different morphological types of non-interacting objects are similar, and then we do not notice differences in H α EWs with morphological types a found by other authors (e.g. Kennicutt 1998). The much higher H α EWs values found for four of the satellites in interaction indicate that their activity is directly related with current interaction process.

The H α EWs were converted in fluxes ($f_{H\alpha}$) following the calibration explained in Section 2; $f_{H\alpha}$ was then converted into absolute luminosity according to $L_{H\alpha} = 4\pi D^2 f_{H\alpha}$. To estimate distances, we took the recessional velocity of the respective parent galaxy (the satellite is more affected by the peculiar velocities). In any case, the difference in the estimated luminosity would be relevant only for a few systems at very low redshift and with comparatively large differences in velocity between the parent and the satellite (NGC 4030b is the extreme case). For the Hubble constant we assumed $H_0 = 72$ km s $^{-1}$ Mpc $^{-1}$.

The H α fluxes and luminosities are presented in Table 2. For the galaxies with H α emission, the luminosities are in the range $\log L_{H\alpha} = 38.85-41.66$ erg s $^{-1}$. The histogram with the distribution of H α luminosities is presented in Figure 6.

To convert $L_{H\alpha}$ to current star formation rates (SFRs), we use the calibration provided by Kennicutt (1998), $\text{SFR} (M_{\odot} \text{ yr}^{-1}) = 7.9 \times 10^{-42} L_{H\alpha}$ erg s $^{-1}$, which assumes a Salpeter (Salpeter 1955) initial mass function between $10^{-1} - 10^2 M_{\odot}$. Because we do not have observations of other Balmer lines (specifically H β) we did not apply any correction for internal extinction. The values obtained for the current SFR are presented in Table 3 column 2). Figure 7 shows SFR as a function of luminosity in the B band. A significant correlation (although with a large scatter) exists. Similar tendency was found in the sample of blue compact galaxies studied by Kong (2004), and with the much large sample of $\approx 10^5$ SDSS galaxies studied by Brinchmann et al. (2004). Four of the interacting satellite galaxies (indicated by filled circles in the figure) show a similar tendency, although they clearly have higher levels of star formation than non-interacting galaxies with similar luminosities.

4.1. Comparison with previous star formation rates estimations

SFRs of some of the objects analyzed in this work have been previously estimated by other authors. In some cases, their SFRs have been estimated from H α measurements in narrow-band images or spectroscopy, while in others, SFRs have been obtained from observations in the far-IR or radio. Below we compare our results with these previous studies compiled from the literature.

- NGC 2718a and NGC 2718b: Mendez et al. (1999) have estimated a luminosity of 40.87 erg s $^{-1}$ for the component NGC 2718b, which is in good agreement with our value of 40.91 erg s $^{-1}$. However, they derived an EW of 260 \AA for the H α emission of this galaxy, which is a factor > 2 larger than our value. Our estimate of H α EW for this galaxy is also ~ 2.5 smaller than that presented by Kong et al. (2002) from long-slit observations. However, our EW and H α luminosities are in very good agreement with the estimates by Gil de Paz et al. (2003), 120 \AA and 40.85 erg s $^{-1}$ respectively. So, considering only the three measurements based on narrow-band imaging, it seems that the three

estimates of the H α luminosities are in agreement, but they are in clear disagreement with EWs derived from long-slit spectra. Although the reason for this discrepancy between the estimates obtained with each technique is unclear, it could be related to the irregular spatial distribution of the H α features. This renders inaccurate the extrapolation of the H α intensity from the area covered by the long-slit of the whole galaxy.

- NGC 5965a₁₋₂: The estimates carried out previously by other authors enclose the H α flux for the whole system. For this, our estimate of the H α flux is $27.2 \times 10^{-14} \text{ erg s}^{-1} \text{ cm}^{-2}$, which is in good agreement with the value of $30 \pm 3 \times 10^{-14} \text{ erg s}^{-1} \text{ cm}^{-2}$ measured by Gil de Paz et al. (2003). For this pair, Bell (2003) obtained an SFR of $0.8 M_{\odot} \text{ yr}^{-1}$ from radio measurement, while Hopkins et al. (2002) obtained 0.8 and $1.7 M_{\odot} \text{ yr}^{-1}$ from observations at $60 \mu\text{m}$ and 1.4 GHz respectively. However, these authors use a different distance to the galaxy (53.2 Mpc) instead of the value 47.6 Mpc that we have used. Converting our results to their distance scale, we would obtain $\text{SFR} = 0.72 M_{\odot} \text{ yr}^{-1}$, which is within 25% of the value derived by these authors from the luminosity at $60 \mu\text{m}$. Given the different uncertainties and assumptions in each of the methods, we consider both estimates to be in very good agreement.

5. Interactions and star formation

Observations and simulations have shown that galaxy interactions and mergers are powerful mechanisms for triggering star formation (e.g. Kennicutt 1998; Donzelli & Pastoriza 1997; Barton et al. 2000; see, however, Bergvall et al. 2003). Lambas et al. (2003) and Alonso et al. (2004) have carried out statistical analyses of star formation in the sample of galaxies of the 2dF survey (Colless et al. 2001), finding that objects with close neighbors tend to have a higher star formation activity than those that are isolated. This tendency is more efficient for pairs situated in low density regions. According to the studies by Sekiguchi & Wolstencroft (1992) and Donzelli & Pastoriza (1997), enhancement of the star formation activity is more likely to take place in both galaxies of the pair but tends to be higher in the fainter component. However, the analysis by Lambas et al. (2003) indicate that a large number of interact-

ing galaxies do not show enhanced star formation activity.

Two basic types of interactions can be differentiated in the halos of giant galaxies; those between parent and satellites, and those between satellites. Both in principle can produce morphological changes and mass losses, and affect the star formation activity in the interacting objects; for instance Knebe et al. (2005) by using N -body simulations have estimated that interactions between satellites can account for $\sim 30\%$ of the total lost masses through their hectic existence.

Gutiérrez et al. (2002) pointed out two clear cases of interaction (NGC 2718a-b, NGC 4541b-e) between pairs of satellites. An additional pair (the two components of NGC 5965a) was also considered by Gutiérrez & Azzaro (2004). A relatively high fraction of other satellites in our sample show morphological signs that could be attributed to present or recent interaction (see Section 3 and Appendix A), but the possible companions have not been accurately identified. Our results confirm that interactions between satellites significantly affect the star formation activity.

According to Gutiérrez & Azzaro (2004) the difference in magnitudes between the two members of the pairs NGC 2718ab, NGC 4541be, and NGC 5965a_{1a2} are $\delta m \sim 1 \text{ mag}$ in the R band. In the first two cases, a high level of H α emission is detected in just one member of the interacting system, NGC 2718b and NGC 4541e, which are brighter components of their respective pairs. The other two galaxies in these pairs, NGC 2718a and NGC 4541b are the only two members of the sample analyzed that do not show H α emission. These two galaxies are also the only objects in our sample that were classified as early types and have been included only as members of the interacting pairs. The filaments and bridges seen in the pairs NGC 2718a-b and NGC 4541b-e do not show H α emission either. We propose that in the case of NGC 2718a the presence of the bridge connecting this galaxy with the companion, and the comparative large amount of gas (see next section) in NGC 2718b are signs of mass transfer from one galaxy to the other. This is probably inhibiting the galaxy formation in the donor and enhancing it in the accreting galaxy. The stripping suffered by NGC 2718a could also be responsible for its morphological evolution toward early-type ob-

jects. The situation is more confuse for the pair NGC4541 b-e, where only one of the two plumes emerging from NGC 4541b seems to point towards NGC 4541e and there are no HI measurements in the literature for any of the two galaxies of the pair.

In the pair NGC 5965a₁-a₂ both members show a high level of star formation, the brighter galaxy (a₁) also being the one that has experienced the more intense SFR activity. In this case, the small projected spatial distance, the absence of tidal streams, or bridges and the elongation of the isophotes through the respective companion seem indicate that these two galaxies are experiencing the first approximation and the gas is being strongly compressed.⁴ We have also computed the H α emission in an aperture enclosing both galaxies and obtained $SFR = 0.576 M_{\odot} \text{ yr}^{-1}$. This is $\sim 5\%$ higher than the result obtained by just adding the H α emission estimated for each component. Although compatible with the uncertainties of the method, this excess could also indicate the presence of some H α residual emission in the intergalactic media. The fact that in each of the interacting pairs the SFR activity is more intense in the brighter component is in disagreement with the results of Donzelli & Pastoriza (1997).

Our sample does not contain clear cases of interactions between satellites and parents, so that it is not possible to estimate the relevance of such interactions to star formation activity. We note, however, that NGC 3154a, which is the object in our sample that has the smaller projected distance from its progenitor (19 kpc), is one of the more active satellites forming stars. However, we do not notice special signs of morphological distortion in this satellite.

We can roughly check if the abundance of interacting pairs found is reasonable according to the expectations of numerical simulations in CDM models. Knebe et al. (2004) have estimated that the mean number of satellites that have at least an encounter per orbit with other satellites depends on halo age, and ranges from $\sim 4\%$ (for old ha-

los) to $\sim 58\%$ (for young halos). These encounters tend to be more frequent and faster in the internal parts of halos. The three interacting pairs found in a sample of ~ 60 satellites studied by Gutiérrez & Azzaro (2004) would then require very low velocity encounters, with interactions lasting $\sim 1/2 - 1/8$ of the orbital period. This seemsto contradict the observed differences in radial velocities ($\sim 50 - 90 \text{ km s}^{-1}$), and projected distances ($\leq 20 \text{ kpc}$) between both members of each pair. However, larger statistical samples are needed to make a more robust assesment.

6. Current vs. past star formation rates

The star formation history for satellites in CDM halos have been considered by Mayer et al. (2001). These author show that high and low surface brightness and galaxies (HSB and LSB respectively) react differently to the interaction with the central galaxy. In LSB satellites bursts of activity occur after each pericentric passage, while in HSB satellites the first burst consumes most of the gas. In both cases the activity is very inhomogeneous over cosmological times. Following the method proposed by van Zee (2001) it is possible to estimate the average star formation rate over the Hubble time from the total mass of stars formed. The resulting $\langle SFR \rangle_{\text{past}}$ for the galaxies in our sample are presented in Table 3 column 3, and are in the range $\sim 0.04 - 1.04 M_{\odot} \text{ yr}^{-1}$. For most of the galaxies, these values are larger than the current star formation rates as estimated from the H α luminosities. The normalized distributions of the current and past SFR are shown in Figure 8. It is worth noting that the current SFR spans a large range of values extending the distribution to very low values. The histogram of $\langle SFR \rangle_{\text{past}}$ looks sharper and shifted to higher values. The ratio between present and average past star formation rates is usually called the birthrate parameter $b = SFR_{\text{current}} / \langle SFR \rangle_{\text{past}}$. The mean value of this parameter is largely conditioned by the high values of the starbursting interacting systems, so we think as more representative of the general distribution, the median, which results 0.68.

The absolute magnitude of each satellite vs. $\log b$ is shown in Figure 9. The region with higher values of the b parameter is occupied by the four starbursting interacting galaxies and by

⁴We consider the two components of NGC 5965a to have velocities of 3357 and 3429 km s^{-1} for NGC 5965a₂ (SBS 1533+574A) and NGC 5965a₁ (SBS 1533+574B) respectively (Izotov, Y. 2005 priv. comm.). Apparently the recessional velocity quoted in the NED database for the component SBS 1533+574B is wrong.

NGC 3154a. The b values for these galaxies are in the range 3–9. We notice a weak trend in the sense that brighter satellites seem to have a comparatively higher current activity; in fact, four of the five brightest galaxies (excluding the interacting systems) have $b \sim 1$, which seems to indicate that these galaxies are still able to maintain now their mean past star formation rate. The global tendency of decline in star formation rate with cosmological time is expected according to simulations by Mayer et al. (2001). The values of b by any of the morphological types (excluding the interacting systems) spread roughly an order of magnitude, which probably indicates a great variety of star formation histories. The distribution of b (see Figure 8) is qualitatively similar to that found by van Zee (2001). We do not notice any clear differences between the different morphological types, but given the small sizes of the sample we have not tried to quantify this accurately.

Another way to compare the relevant time scales for the star formation evolution is by computing how much time (t_{form}) the galaxy would have needed to form all the stellar content at the current star rate, and what is the maximum time (t_{gas}) that the galaxy can continue forming stars at the current rate. The analysis of this in conjunction with optical luminosities and current star formation allow a first approximation to the evolution of the galaxy over cosmic times. An accurate limit for t_{gas} can be estimated simply dividing the current gas content by the current star formation rate. This of course would correspond to an ideal case in which all the gas would be converted into stars, and no losses or accretion occurred. Using the LEDA database,⁵ we have compiled the existing HI measurements as a way to estimate the gas content in each galaxy. These are presented in Table 3 column 4. The values of t_{gas} indicate that the current gas content would be enough to fuel the star formation at the current star formation rate at least during another Hubble time. For about one third of the galaxies t_{form} exceeds the Hubble time, so that we conclude again that on average the star formation rate was higher in the past. As expected, the starbursting galaxies NGC 2718b, NGC 4541e and NGC 5965a₁, and NGC 5965a₂ are among the objects with the low-

est formation times (also NGC 3154a, which is the satellite galaxy in our sample closest to their parent).

Previous studies (e.g., Casoli et al. 1996) have shown that star formation rate in spiral galaxies is correlated with the mass of molecular and atomic gas. Our results confirm that relation as illustrated in Figure 10. The correlation extends one and two orders of magnitude in gas mass and star formation rate respectively. NGC 2718b, one of the interacting galaxies have the largest SFR in the sample and also one of the galaxies with higher gas content. This seems reinforce the scenario of significant accretion of gas from NGC 2718a as outlined in previous section.

Figure 11 presents t_{gas} vs. t_{form} , for our sample of satellite galaxies and compares these time scales with those for other four samples taken from the literature: the Sculptor group dIrrs studied by Skillman et al. (2003), the Local Group dIrrs of Mateo (1998), the gas-rich low surface brightness galaxies studied by van Zee et al. (1997), and the isolated dIrrs of van Zee, (2000, 2001). The figure shows a clear direct correlation between both time scales. The range of magnitudes and the selection effects are different for each sample so that it is difficult to extract statistical conclusions, although all the samples tend to follow common tendencies. The lower limit in t_{form} in our sample is ~ 1 Gyr and

7. Summary

We have carried out a detailed analysis of narrow-band observations of the H α emission in a sample of 31 satellites orbiting giant spiral isolated galaxies. The objects studied span the range $-19 < M_B < -15$ mag. and were selected according to the relative brightness (at least 2.2 magnitudes fainter than their parents), projected distances (< 500 kpc) and relative velocity (< 500 km s⁻¹) from the primaries. We have presented imaging and photometry in a narrow filter band covering the position of the H α line. The results can be summarized as follows:

- In all the spirals and irregular satellites (29 objects) we detected H α fluxes above $1.15 \cdot 10^{-14}$ erg s⁻¹ cm⁻². The inferred current star formation rates are in the range $0.006\text{--}3.66 M_{\odot} \text{ yr}^{-1}$.
- There are three cases of clear interacting

⁵<http://leda.univ-lyon1.fr/>

pairs. Four of the galaxies in these pairs are among the objects with higher star-forming activity. In contrast, the only two galaxies of the sample that are not forming stars are also members of these pairs. We do not detect H α emission in the filaments associated with these interactions.

- The object with a largest current star formation rate (apart of the interacting systems) corresponds to the satellite galaxy NGC 3154a, which has the smallest projected distance from its progenitor (19 kpc) and the SFR could be due to interaction with the parent galaxy.

- The median of the birth parameter b is 0.68, indicating a fall in activity with cosmic time, assuming perfect efficiency the current gas content of the galaxies is enough to fuel this activity for more than another Hubble time.

Appendix A

Description of the H α emission maps of each galaxy:

- NGC 488c: This is a low surface brightness irregular galaxy in which we notice four main knots with H α emission located in the outer parts of the galaxy.

- NGC 772b: What seems a bright foreground star is projected through the E side of the galaxy. The H α emission is concentrated in a few discrete spots, the two brightest being situated NE.

- NGC 772c: There are diffuse and discrete H α emission features. The two brightest spots are situated roughly symmetrically with respect to the galactic center.

- NGC 1517a: There are about ten H α regions, which are particularly bright in the external parts of the galaxy. Two of the H α features through the W are clearly differentiated from the main body of the disk.

- NGC 1620a: The galaxy is irregular with two–three plumes emerging from the W. In one of these plumes there are a few discrete features with H α emission. The rest of the emission is concentrated in a few features distributed over the full galaxy,

- NGC 1961a: A few clumpy small and faint structures are detected in the image after continuum subtraction.

- NGC 1961b: It is a luminous spiral satellite galaxy which has a bright point-like structure close

to the center. The H α continuum subtracted image shows a diffuse H α emission with a few over-imposed features concentrated along two chains in direction NE–SW enclosing the central part of the galaxy. The brightest spot at 3.8 arcsec from the geometrical center was suspected to be a foreground star but it is the dominant component in the continuum free image, so we think it is a real galactic feature (or an intruder) experiencing a strong starburst.

- NGC 1961c: This galaxy is a face-on spiral, which has a very rich structure in H α emission with several extended features. The two more intense are situated in the geometrical center and in a spot NW which is also obvious in the R -band image.

- NGC 2424b: This is a very irregular galaxy which shows a clumpy structure in the broad-band image. The H α continuum free image shows about six discrete spots, being the most intense the one located to the SW of the galactic center.

- NGC 2718a and NGC 2718b: These galaxies are a clear pair of interacting satellites and have a sharp and very straight bridge ($\approx 92'' = 25$ kpc) connecting both galaxies. Close to NGC 2718a, and perpendicular to the main axis there are what could be a small companion. The continuum-free image shows that the only component with H α emission is NGC 2718b which has 3–4 intense knots.

- NGC 2775a: The two brightest H α emission features are projected very close and are only partially resolved. The position coincides with the geometrical center of the galaxy. Most of the remaining emission is concentrated in a few spots situated to the SE of the galaxy.

- NGC 2775c: This galaxy shows an intense H α emission with a very irregular spatial distribution concentrated mainly in the northern part. A differentiated feature is to the SE of the galaxy. The broad-band image shows in that position a plume emerging from the main body of the galaxy.

- NGC 2916a: The H α subtracted image shows an intense and diffuse structure along the major axis. There are two less intense knots situated in the E and W edges of the galaxy.

- NGC 3043a: There is an extended diffuse structure where it is possible to distinguish at least five differentiated regions distributed through the

full area (but avoiding the geometrical center) of the galaxy.

- NGC 3154a: The $H\alpha$ emission is spread over the full projected area of the galaxy in the form of diffuse emission and discrete knots. The most intense spot is located at the geometrical center. This is the galaxy in our sample which has the smallest projected distance from its progenitor and (apart from the interacting galaxies), the one with largest $H\alpha$ luminosity. Although this could be related with a possible interaction with its parent, we do not notice relevant signs of geometrical distortions in the satellite.

- NGC 3735a: The $H\alpha$ emission is concentrated in the E side of the galaxy. In particular, there a bright feature at the geometrical center and a few other less intense features in structures resembling arms. In the broad-band image, there is some evidence of a tail connecting this galaxy and another smaller one of unknown redshift situated to the NE. However, this last galaxy does not show any $H\alpha$ emission.

- NGC 4030b: The majority of the $H\alpha$ emission is concentrated in four discrete spots. One is located at the center, and another is situated NW coincident with what we have identified as a possible small interacting galaxy. Unfortunately, the redshift of this last object is unknown.

- NGC 4541a: The broad-band image shows a spiral edge-on galaxy with two small structures perpendicular to the major axis on both edges. The $H\alpha$ continuum-free image shows a diffuse structure that extends over most of the projected area of the galaxy, and some very clumpy structure. This emission seems to be asymmetrically distributed through the SW, where one of the features mentioned in the broad-band image shows clear evidence of $H\alpha$ emission. We think that this could be a small interacting object that could be enhancing the star formation in the neighboring regions of the main galaxy.

- NGC 4541b and NGC 4541e: This pair of galaxies are separated by ~ 41 arcsec. The galaxies have morphological types E and S0/Sa respectively. In the broad-band image there are two tidal tails emerging from NGC 4541b. One of them is pointing directly to NGC 4541e and it seems clear that its origin is the interaction with this galaxy. The other, pointing nearly in the oppo-

site direction, seems more extended and is possibly the relic of a previous passage of this galaxy near NGC 4541e. The continuum-subtracted $H\alpha$ image shows an intense structure in NGC 4541e, while NGC 4541b has no $H\alpha$ emission. The $H\alpha$ emission in NGC 4541e seems to be composed of at least four major clumps located in the main body of the galaxy. A few faint features seem to follow two arms in approximately opposite directions.

- NGC 4725a: This is the largest satellite in our sample. The morphology corresponds to a late spiral with clear signs of distortions and possibly dust obscuration. In particular, a plume emerges in the NE direction. The $H\alpha$ emission is concentrated along the major axis with two bright spots, one approximately in the geometric center and the other to the SW.

- NGC 5248a: The $H\alpha$ features are distributed over the full projected area of the galaxy in about a dozen faint independent features.

- NGC 5248b: The brightest spot is located at the geometrical center with a number of diffuse structures distributed through the disk.

- NGC 5899a: The galaxy shows a rich structure with diffuse $H\alpha$ features extending over the disk and three major discrete features, one in the center and the other two in direction NW. A line of diffuse $H\alpha$ emission seems to cross the galaxy in a direction perpendicular to the major axis. We think this is an example of extra-planar diffuse ionized gas.

- NGC 5962d: The $H\alpha$ emission features are distributed in numerous discrete features in the disk, avoiding the central part of the galaxy.

- NGC 5965a: This corresponds really to two close galaxies as was noted by Zwicky (1971) and Gutiérrez & Azzaro (2004), separated by ~ 7.4 arcsec. Following the notation of that paper, we denote them as NGC 5965a₁ and NGC 5965a₂ (other authors have denoted the two members of this pair as SBS 1533+574b and SBS 1533+574a respectively). The continuum-subtracted image shows that both components have $H\alpha$ emission. In the NW component it is possible to recognize at least two irregular features. The isophotes of the NW component are elongated in the direction of the companion. Additionally, the system is surrounded by a diffuse halo.

- NGC 6181a: This is a late-type spiral with evident signs of distortion in the broad-band image. The H α continuum free image shows a complex structure dominated by a bright discrete feature which shows at least three bright spots, It seems that this spot corresponds to a structure which is differentiated from the main body of the galaxy and could correspond to a minor merger.

- NGC 7137a: The H α emission is concentrated in two extended features situated in the E side of the galaxy. The brightest runs in direction perpendicular to the main axis.

- NGC 7678a: This nice face-on spiral galaxy has H α emission in the form of discrete features in the center and in a ring surrounding the galaxy and approximately tracing the spiral structure. A small galaxy is located very close by to the NW. This does not show any H α emission. The main H α -emitting regions are located in two extended regions situated in the NE part of the galaxy. Two plumes of diffuse material seem connect these two structures with the main body of the galaxy. We think that they could be two separate structures in the process of strong interaction with the main galaxy.

We thank S. Laine who read the manuscript and given us very useful hints and comments. We thank also F. Prada who participated in the first stages of this project. E. D. Skillman has kindly provided the data used for the comparison presented in Fig.11. S. A. was supported by the Consejo Nacional de Investigaciones Científicas y Técnicas (CONICET), and by a Marie Curie Fellowship of the European Community program MEST-CT-2004-504604.

REFERENCES

- Alonso, M. S., Tissera, P. B., Coldwell, G., & Lambas, D. G. 2004, MNRAS, 352, 1081
- Bell, E. F., 2003, ApJ, 586, 794
- Bergvall, N., Laurikainen, E., & Aalto, S. 2003, A&A, 405, 31
- Bertin, E. & Arnouts, S, 1996, A&AS, 117, 393
- Barton, E. J., Geller, M. J., & Kenyon, S. J. 2000, ApJ, 530, 660
- Brinchmann, J., Charlot, S., White, S. D. M., Tremonti, C., Kauffmann, G., Heckman, T., & Brinkmann, J. 2004, MNRAS, 351, 1151
- Casoli, F., Dickey, J., Kazes, I., Boselli, A., Gavazzi, P., & Baumgardt, K. 1996, A&A, 309, 43
- Colless, M. et al. 2001, MNRAS, 328, 1039
- Dijkstra, M., Haiman, Z., Rees, M. J., & Weinberg, D. H. 2004, ApJ, 601, 666
- Donzelli, C. J., & Pastoriza, M. G. 1997, ApJS, 111, 181
- Gil de Paz, A., Madore, B. F., & Pevunova, O. 2003, ApJSS, 147, 29
- Gutierrez, C. M., Azzaro, M., & Prada, F. 2002, ApJS, 141, 61
- Gutierrez, C.M., & Azzaro, M. 2004, ApJSS, 155, 395
- Hopkins, A. M., Schulte-Ladbeck, R. E., Drozdovsky, I. O., 2002, AJ, 124, 862
- Kauffmann, G., White, S. D. M. & Guiderdoni, B., 1993, MNRAS, 264, 210
- Kennicutt, R. C. Jr. 1992, ApJSS, 79, 255
- Kennicutt, R. C. Jr. 1998, ARA&A, 36, 189
- Klypin, A., Kravtsov, A.V., Valenzuela, O., & Prada, F. 1999, ApJ, 522, 82
- Knebe, A., Gill, S. P. D., & Gibson, B. K. 2004, PASA, 21, 216
- Knebe, A., Power, C., Gill, S. P. D., & Gibson, B. K. 2005, MNRAS, astro-ph/0507380
- Kong, X., Cheng, F. Z., Weiss, A., & Charlot, S. 2002, A&A 396, 503
- Kron, R. G., 1980, ApJS, 43, 305
- Lambas, D., G., Tissera, P. B., Alonso, M. S., & Coldwell, G. 2003, 346, 1189
- Mateo, M. L. 1998, ARA&A, 36, 435
- Mendez, D. I., Esteban, C. & Balcells, M. 1999, AJ, 117, 1229

- Moore, B., Ghigna, S., Governato, F., Lake, G.,
Quinn, T., Stadel, J., & Tozzi, P. 1999, ApJ,
524, L19
- Oke, J. B., 1990, AJ, 99, 1621
- Salpeter, E. E., 1955, ApJ, 121, 161
- Sekiguchi, K., & Wolstencroft, R. D. 1992, MN-
RAS, 255, 581
- Skillman, E. D., Cote, S., & Miller, B. W. 2003,
AJ, 125, 593
- Somerville, R., 2002, ApJ, 572, 23
- van Zee, L. 2000, AJ, 119, 2757
- van Zee, L. 2001, AJ, 121, 2003
- van Zee, L., Haynes, M. P., & Salzer, J. J., 1997,
AJ, 114, 2479
- Willman, B., Governato, F., Dalcanton, J. J.,
Reed, D., & Quinn, T. 2004, MNRAS, 353, 639
- White, S. D. M., & Rees, M. J. 1978, MNRAS,
183, 341
- Zaritsky, D., Smith, R., Frenk, C., & White, S. D.
M. 1997, ApJ, 478, 39
- Zwicky, F. 1971, "Catalogue of selected Com-
pact Galaxies and of Post-eruptive Galax-
ies", Guemligen, Switzerland: F. Zwicky

TABLE 1
LOG OF THE OBSERVATIONS

Galaxy	Epoch	t_R (s)	$t_{H\alpha}$ (s)	FWHM R (arcsec)	FWHM $H\alpha$ (arcsec)	Cal. star	$H\alpha$ Filter
NGC 488c	Dec 2001	1200	3x1800	2.2	1.8	BD+75 325	663
NGC 772b	Dec 2001	1200	3x1800	1.5	1.6	BD+75 325	663
NGC 772c	Dec 2001	1200	3x1800	1.3	1.7	GD 50	663
NGC 1517a	Dec 2001	900	3x1800	1.6	1.8	BD+75 325	663
NGC 1620a	Dec 2001	180	3x1800	1.6	2.1	BD+75 325	663
NGC 1961a	Dec 2001	900	3x1800	1.6	1.6	G193-74	663
NGC 1961b	Dec 2001	1200	3x1800	1.7	1.4	BD+75 325	663
NGC 1961c	Dec 2001	1200	3x1800	1.1	1.2	BD+75 325	663
NGC 2424b	Dec 2001	1200	3x1800	1.6	1.6	—	663
NGC 2718a	May 2002	900	3x1800	1.5	1.1	Feige 34	663
NGC 2718b	May 2002	900	3x1800	1.5	1.1	Feige 34	663
NGC 2775a	Dec 2001	300	3x1800	1.2	1.5	BD+75 325	658
NGC 2775c	Dec 2001	1200	3x1800	1.3	1.4	BD+75 325	658
NGC 2916a	Dec 2001	1200	3x1800	1.7	1.5	BD+75 325	663
NGC 3043a	Dec 2001	1200	3x1800	1.6	1.2	BD+75 325	663
NGC 3154a	Dec 2001	1200	3x1800	1.1	1.1	BD+75 325	673
NGC 3735a	Dec 2001	1200	3x1800	1.2	1.4	BD+75 325	663
NGC 4030b	May 2002	1200	3x1800	1.4	1.7	Feige 66	658
NGC 4541a	May 2002	1200	3x1800	1.6	1.6	Feige 34	673
NGC 4541b	May 2002	1200	3x1800	1.6	1.6	Feige 34	673
NGC 4541e	May 2002	1200	3x1800	1.6	1.6	Feige 34	673
NGC 4725a	May 2002	1200	3x1800	1.2	1.3	BD+33 2642	658
NGC 5248a	May 2002	1200	3x1800	1.1	1.2	BD+33 2642	658
NGC 5248b	May 2002	600	3x1800	1.8	1.7	Hz 44	658
NGC 5899a	May 2002	1800	3x1800	1.4	1.4	BD+33 2642	663
NGC 5962d	May 2002	1200	3x1800	1.1	1.3	BD+33 2642	663
NGC 5965a ₁	May 2002	600	3x1800	1.4	1.2	BD+33 2642	663
NGC 5965a ₂	May 2002	600	3x1800	1.4	1.2	BD+33 2642	663
NGC 6181a	May 2002	600	3x1800	1.2	1.2	BD+33 2642	663
NGC 7137a	Dec 2002	500	3x1200	2.2	2.3	—	658
NGC 7678a	Dec 2001	1200	3x1800	1.4	1.6	BD+75 325	663

TABLE 2
 $H\alpha$ EQUIVALENT WIDTH, FLUXES AND $H\alpha$ LUMINOSITIES

Galaxy	r_p (kpc)	$EW_{H\alpha}$ (Å)	$H\alpha$ Flux (10^{-14} ergs cm^{-2} s^{-1})	$\log L(H\alpha)$ (ergs s^{-1})
NGC 488c	116	8.07	1.15	39.13
NGC 772b	390	13.97	2.15	39.48
NGC 772c	429	15.19	4.63	39.81
NGC 1517a	130	23.76	9.33	40.41
NGC 1620a	227	8.03	2.75	39.89
NGC 1961a	214	6.89	7.97	40.45
NGC 1961b	139	15.01	9.90	40.55
NGC 1961c	120	28.42	29.00	41.01
NGC 2424b	182	35.52		
NGC 2718a	102	-11.64		
NGC 2718b	82	118.58	23.80	40.91
NGC 2775a	401	23.99	9.53	39.61
NGC 2775c	64	19.26	21.40	39.96
NGC 2916a	71	14.01	2.66	39.93
NGC 3043a	263	38.72	4.02	39.92
NGC 3154a	19	84.40	13.00	41.11
NGC 3735a	192	3.54	2.01	39.53
NGC 4030b	414	23.03	1.46	38.85
NGC 4541a	193	22.89	5.48	40.78
NGC 4541b	228	-1.29		
NGC 4541e	217	101.22	42.10	41.66
NGC 4725a	132	11.41	49.80	40.22
NGC 5248a	150	9.05	3.78	39.06
NGC 5248b	164	12.33	2.76	38.93
NGC 5899a	106	19.14	40.80	40.79
NGC 5962d	89	6.80	3.58	39.50
NGC 5965a ₁	532	440.68	16.50	40.64
NGC 5965a ₂	532	102.03	9.41	40.40
NGC 6181a	257	30.49	46.40	40.78
NGC 7137a	64	25.21	2.24	39.17
NGC 7678a	165	18.15	9.36	40.42

*Observation for NGC 2424a were not taken in photometric conditions.

TABLE 3
HI MASS, STAR FORMATION PROPERTIES AND TIME SCALES

Galaxy	SFR ($M_{\odot} \text{ yr}^{-1}$)	$\langle \text{SFR} \rangle_{Past}$ ($M_{\odot} \text{ yr}^{-1}$)	$\log M_{HI}$ (M_{\odot})	t_{gas} (Gyr)	t_{form} (Gyr)
NGC 488c	0.011	0.048	8.75	51.9	12.9
NGC 772b	0.024	0.044	8.78	25.1	5.8
NGC 772c	0.051	0.107	8.80	12.4	5.1
NGC 1517a	0.206	0.290	9.57	17.9	2.7
NGC 1620a	0.062	0.149	9.35	35.5	10.7
NGC 1961a	0.225	0.867	9.73	23.5	12.9
NGC 1961b	0.279	0.447			5.5
NGC 1961c	0.817	0.938			3.6
NGC 2424b		0.048	9.05		
NGC 2718a		0.221			
NGC 2718b	0.640	0.081	9.50	4.8	1.8
NGC 2775a	0.032	0.050	9.06	37.6	13.1
NGC 2775c	0.072	0.123	8.74	7.8	8.4
NGC 2916a	0.067	0.285	9.34	32.5	17.2
NGC 3043a	0.066	0.073			
NGC 3154a	1.016	0.347			1.5
NGC 3735a	0.027	0.222			36.1
NGC 4030b	0.006	0.132	8.74	95.0	128.7
NGC 4541a	0.476	0.486			7.3
NGC 4541b		0.382			
NGC 4541e	3.659	1.043			1.0
NGC 4725a	0.132	0.336	9.21	12.0	12.6
NGC 5248a	0.009	0.041	8.82	70.6	19.9
NGC 5248b	0.007	0.057	8.45	41.7	27.3
NGC 5899a	0.489	0.434	9.56	7.3	4.5
NGC 5962d	0.025	0.230	8.56	14.4	35.1
NGC 5965a ₁	0.350	0.132			1.7
NGC 5965a ₂	0.200	0.058			1.3
NGC 6181a	0.476	0.421	9.36	4.8	3.8
NGC 7137a	0.012	0.024	8.80	54.0	7.5
NGC 7678a	0.208	0.400	9.39	11.5	6.7

*HI data were collected from the LEDA catalogue

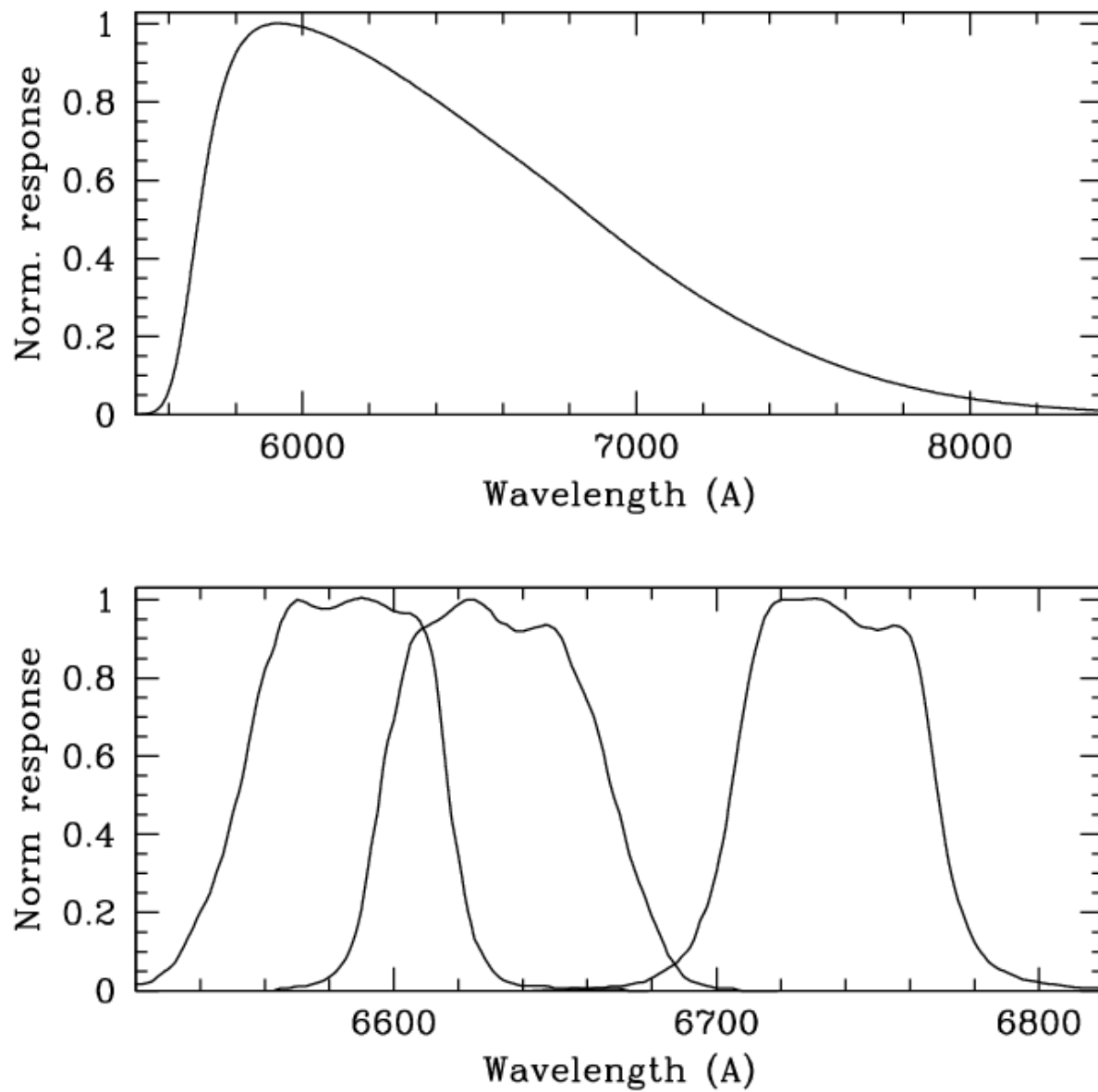


Fig. 1.— Normalized response of the R broad band filter (*top*), and the three narrow band filters (*bottom*) used during the observations presented in this paper.

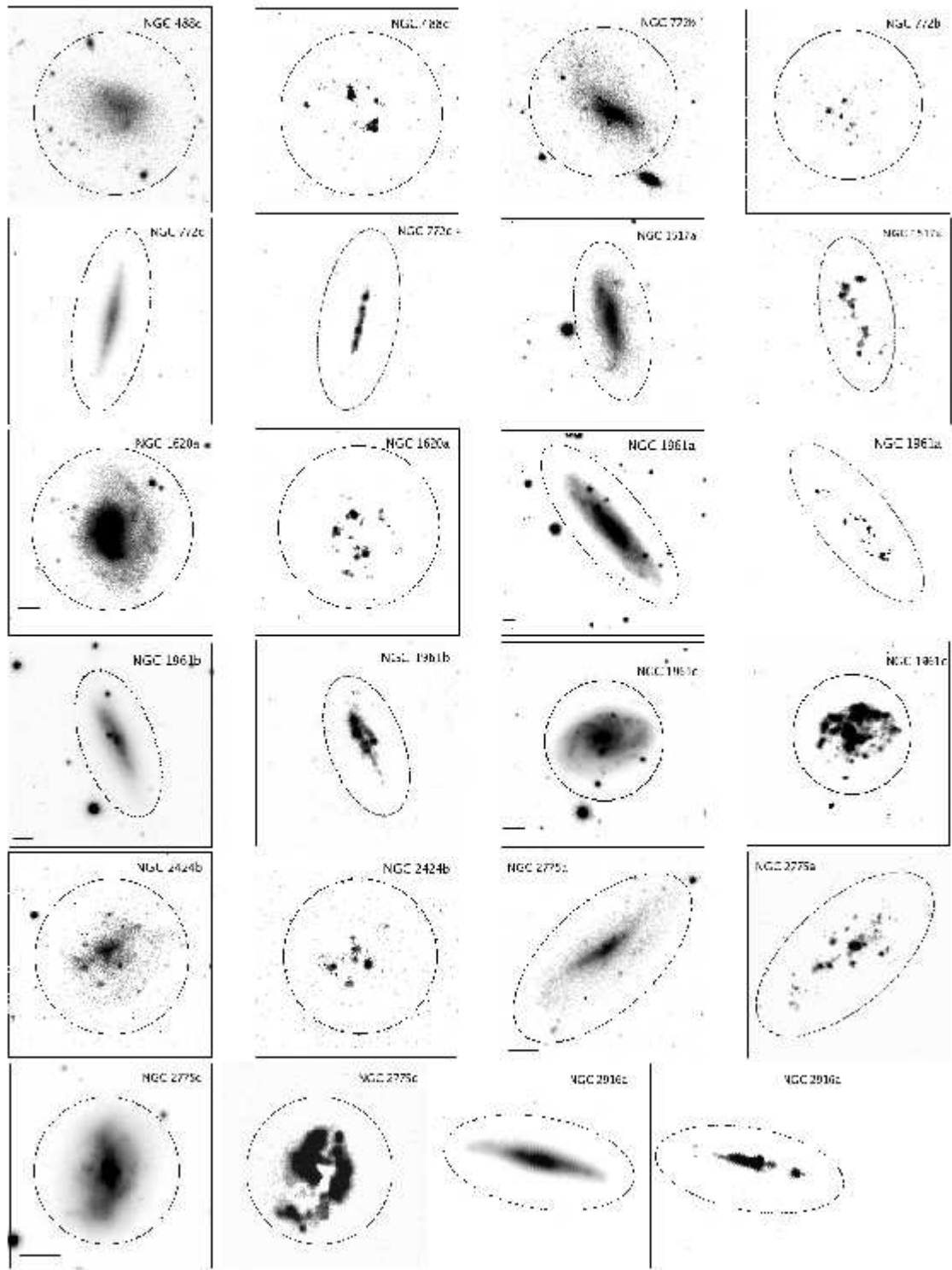


Fig. 2.— Images of the sample of objects analysed in this work. For each object are presented the R-band and H α images after continuum subtraction. North is up and east to the left. The small line at the bottom is scaled to an angular size of 10 arcsecs.

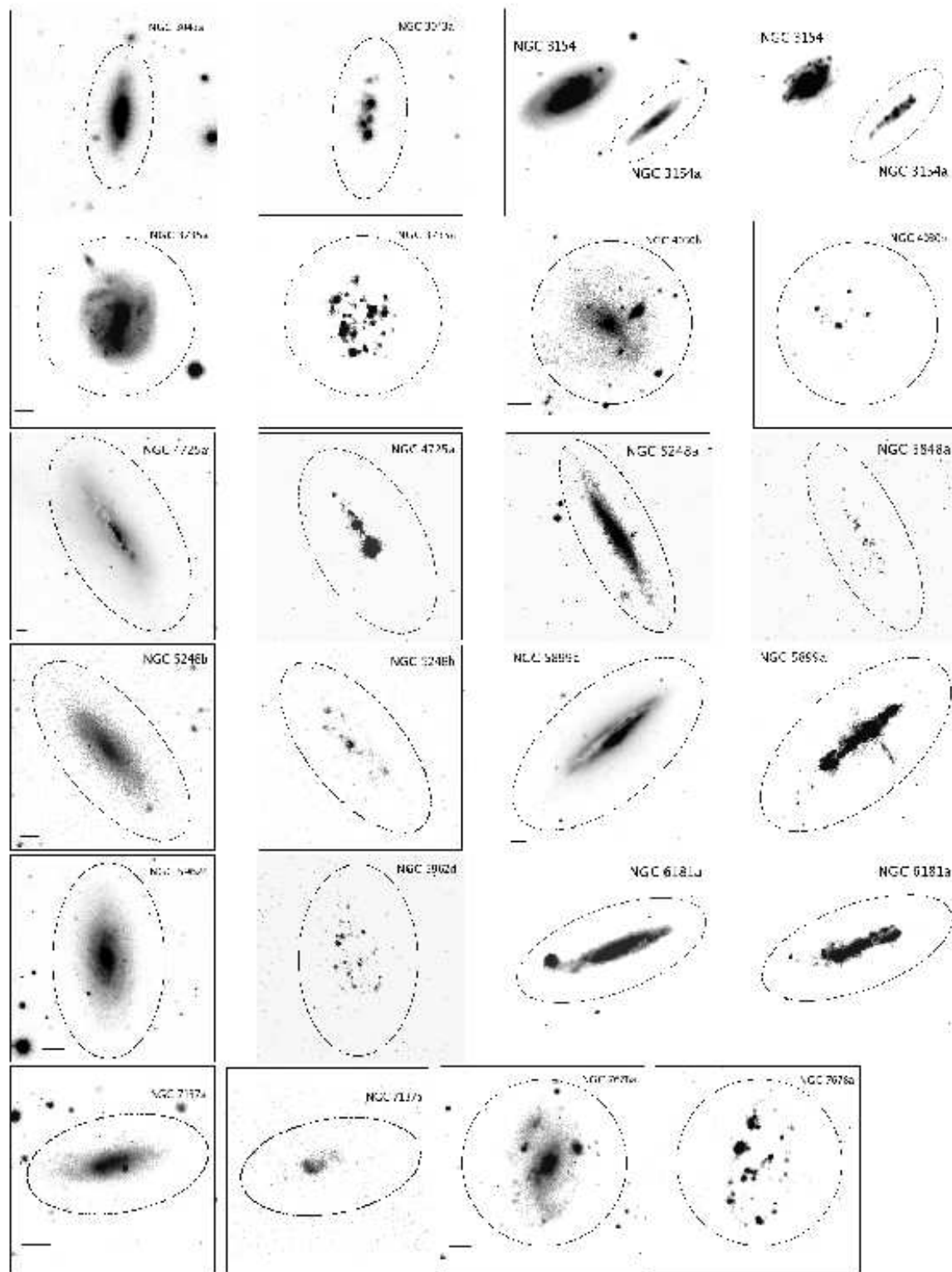


Fig. 3.— Cont.

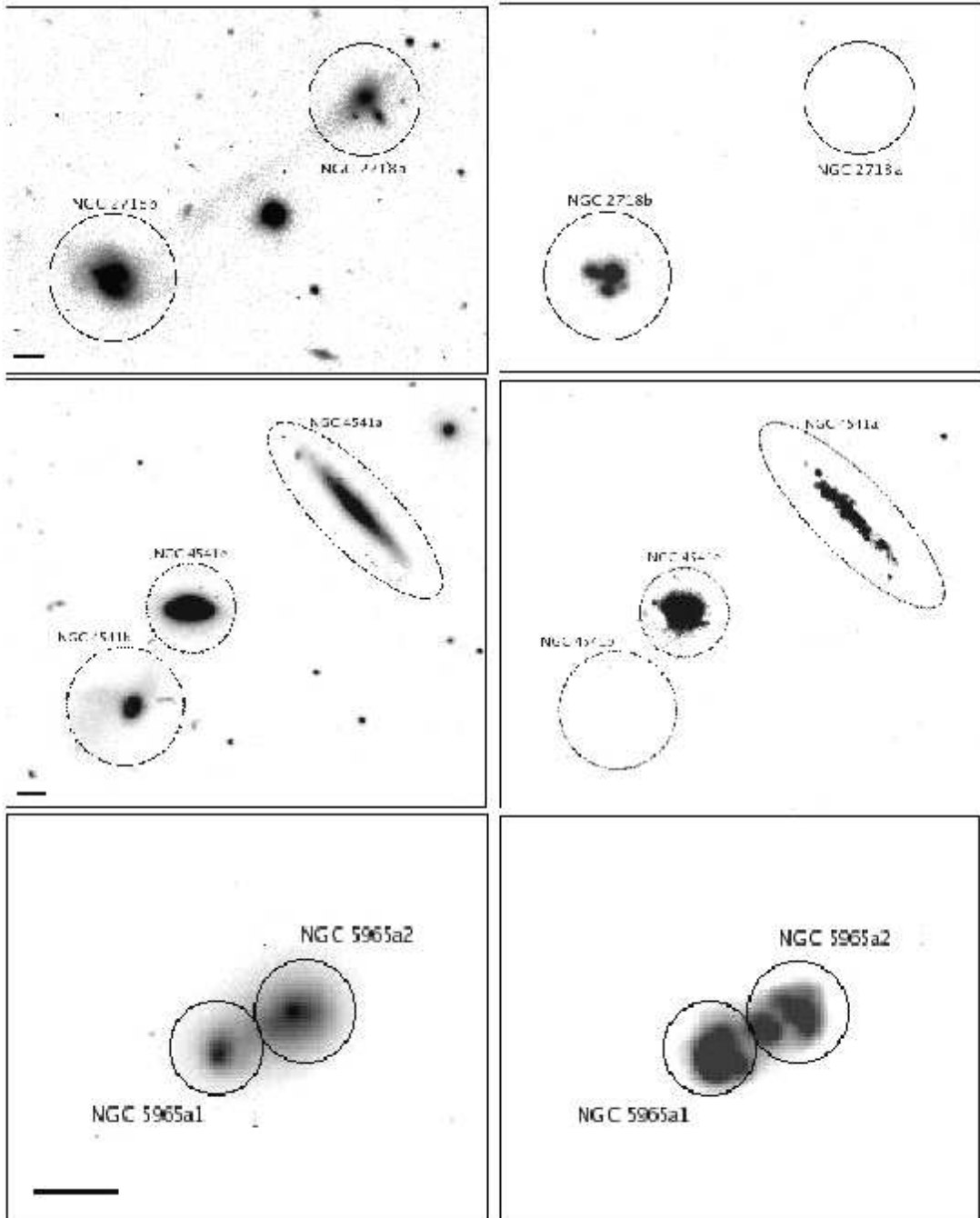


Fig. 4.— Idem for the three pairs of interacting satellite galaxies: NGC2718a-b, NGC4541a, NGC4541b-e and NGC5965a₁-a₂.

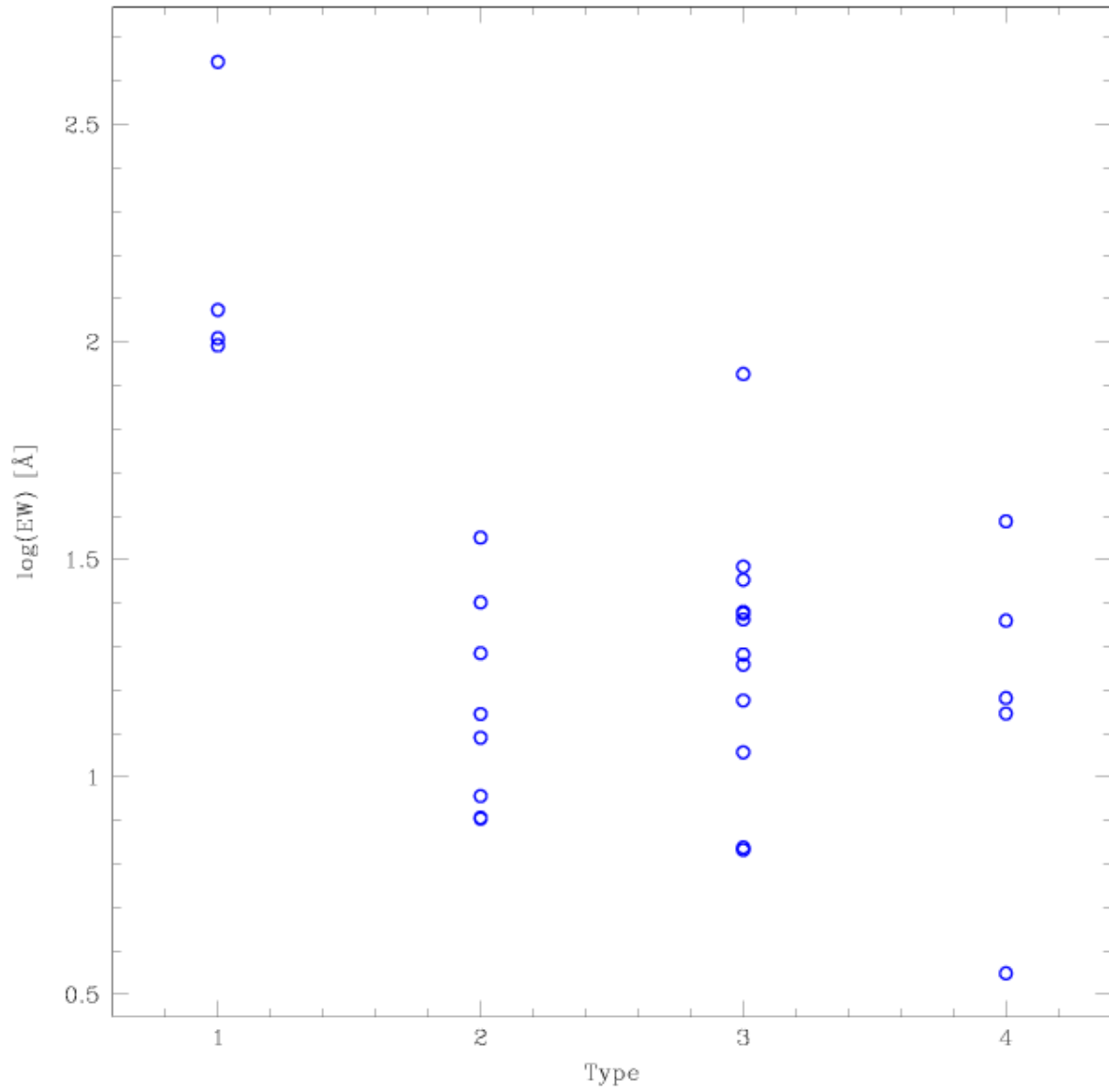


Fig. 5.— $H\alpha$ equivalent widths as a function of the galactic type: (1) Objects in interaction, (2) Irregular, (3) Sb/Sc and (4) Sa.

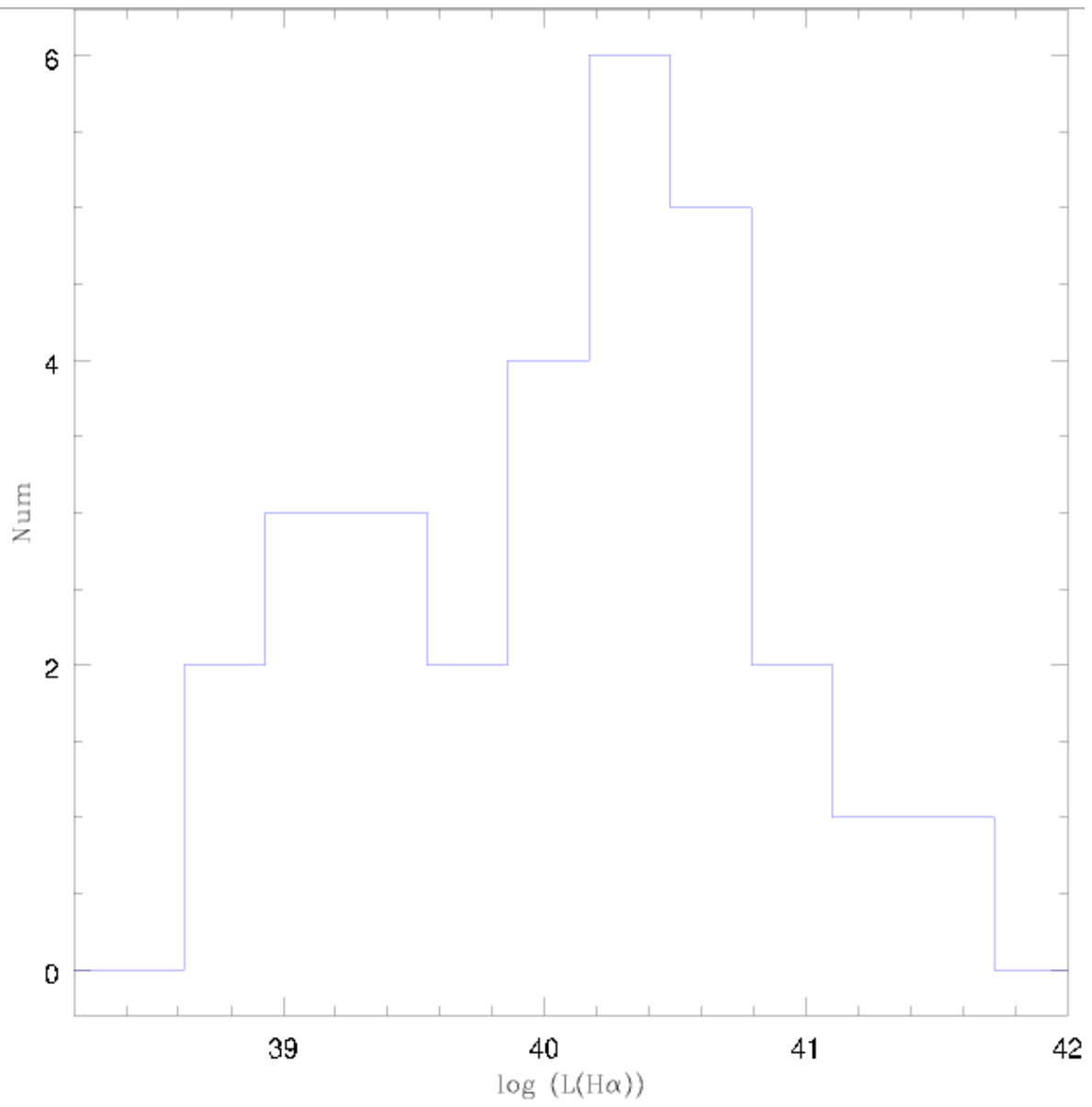


Fig. 6.— Distribution of $H\alpha$ luminosities for the sample of satellite galaxies analysed in this paper.

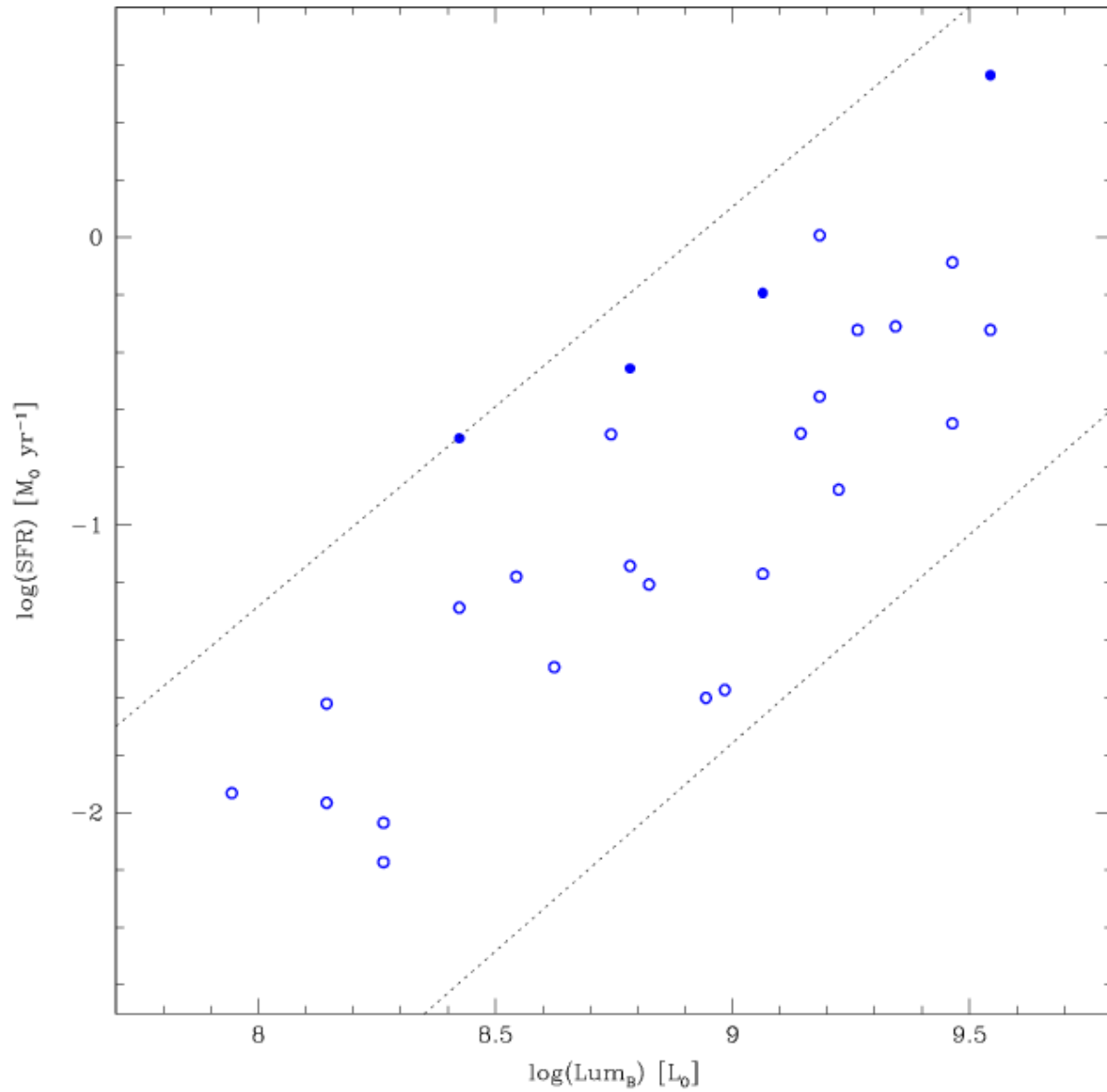


Fig. 7.— Current star formation rate, SFR , estimated from the $H\alpha$ luminosities, as a function of luminosity in the B – band. Objects in interaction have been indicated by a filled circle.

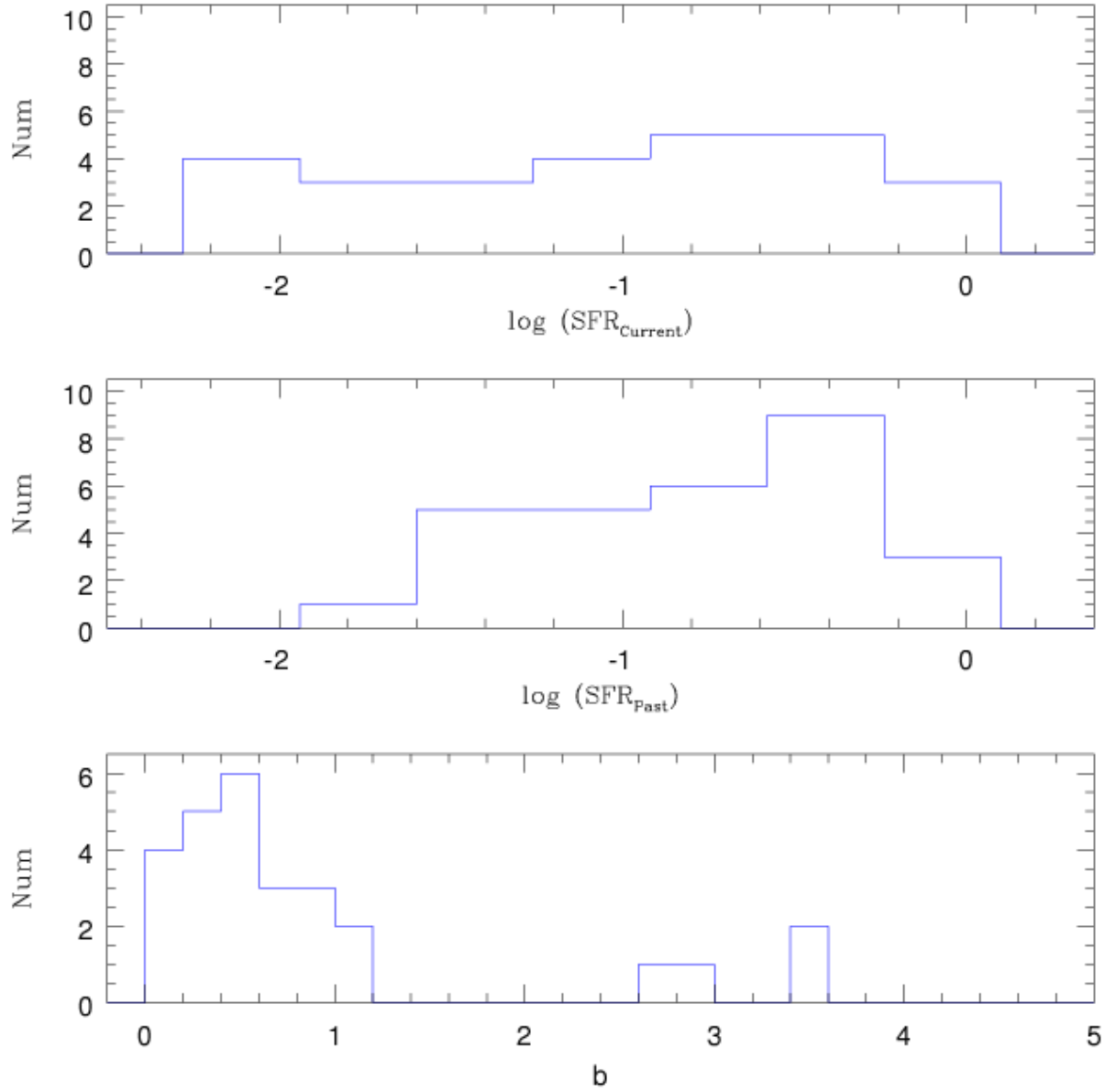


Fig. 8.— Distribution of current (*top*) and past (*medium*) star formation rates, for the sample of satellite galaxies analysed in this paper. The bottom box shows the distribution of stellar birthrate parameter, $b = \text{SFR}_{\text{Current}} / \langle \text{SFR} \rangle_{\text{Past}}$.

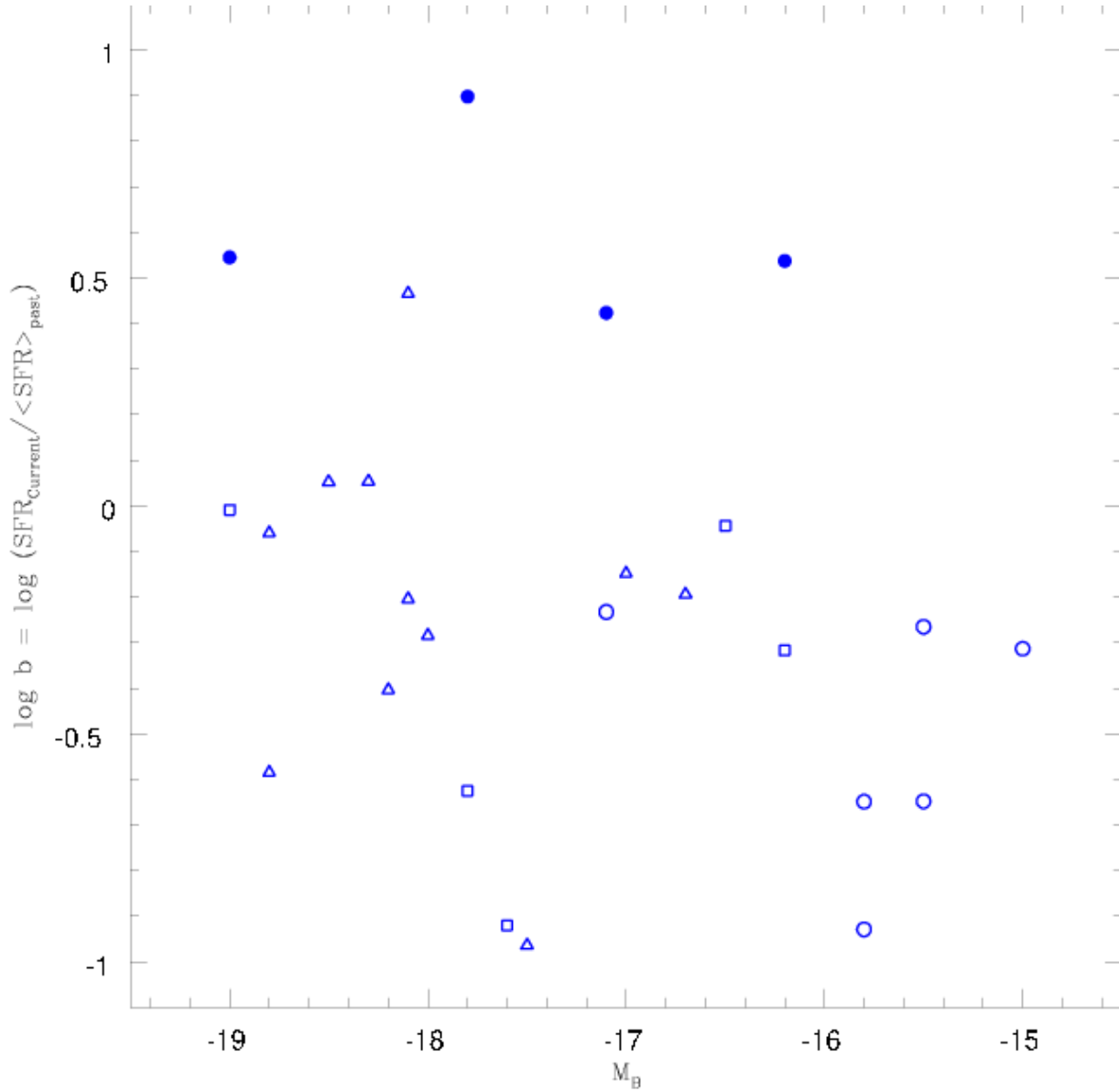


Fig. 9.— Stellar birthrate parameter as a function of the absolute magnitude (M_B), in satellite galaxies for different Hubble morphological types: Irregulars (*open circles*), Sb/Sc (*open triangles*) and Sa (*open squares*). Interacting galaxies are indicated by filled symbols.

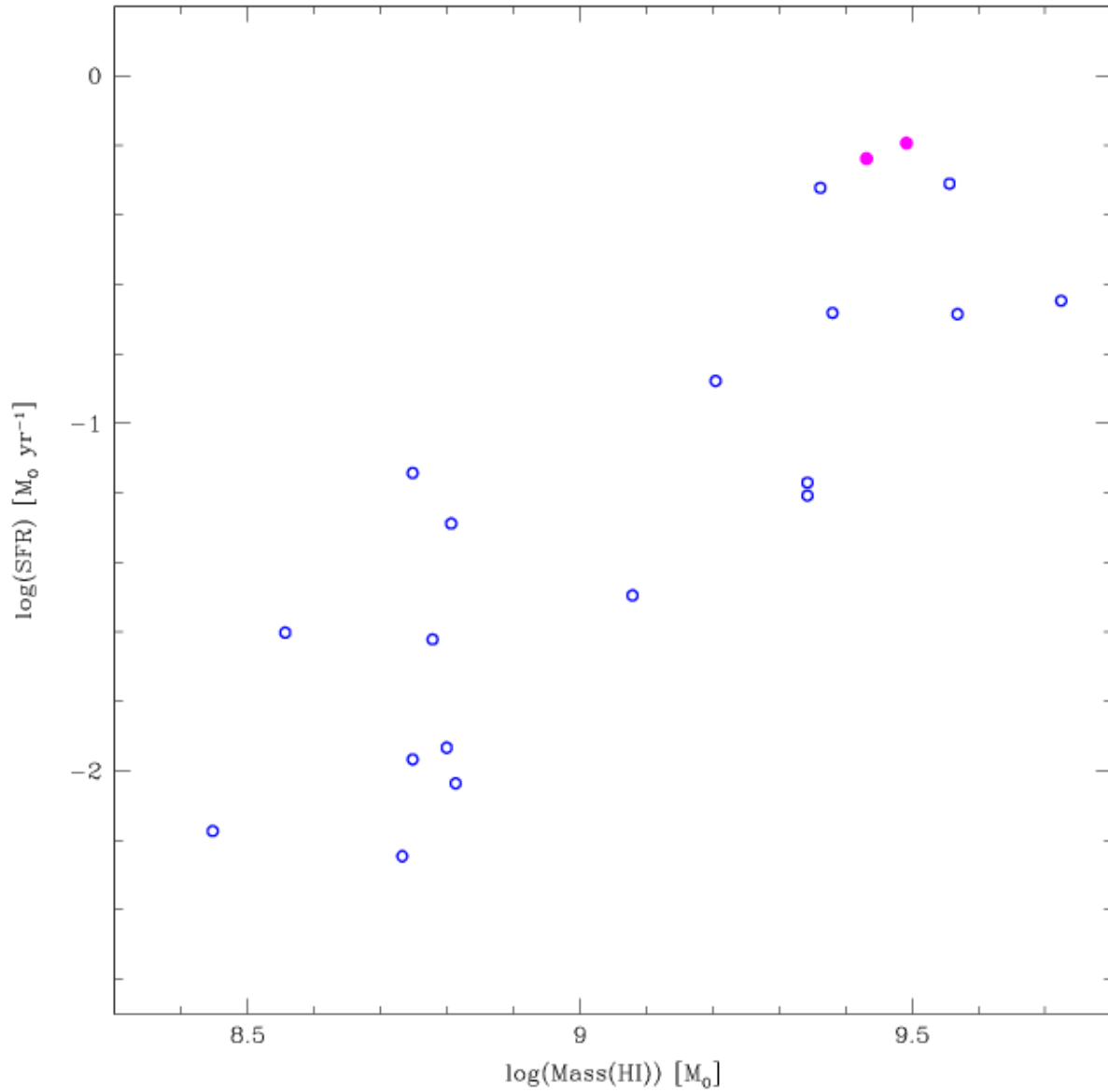


Fig. 10.— Current star formation rate, SFR , estimated from $H\alpha$ measurement, vs. HI mass of the gas. Interacting galaxies, NGC 2718b and NGC 5965a (computed in an aperture enclosing both galaxies, NGC 5965a₁ and a₂), are indicated by filled symbol.

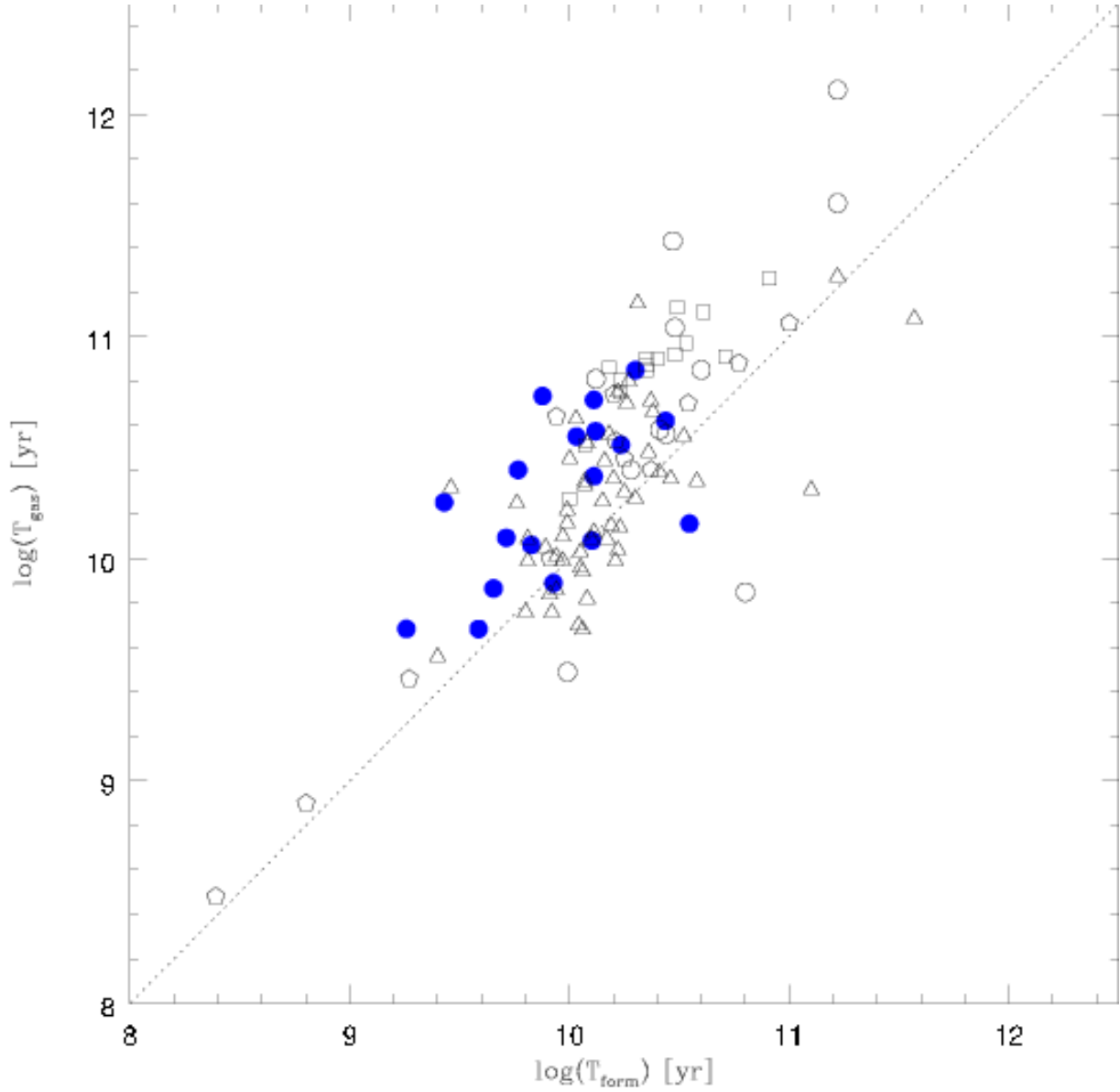


Fig. 11.— Comparison between the ratio of the gas mass to the current SFR (T_{gas}) and the ratio of the luminosity to the current SFR (T_{form}), for the satellite galaxies (filled circles), and four samples taken from the literature: the Sculptor group dIrrs studied by Skillman et al. (2003) (open circles), the Local Group dIrrs of Mateo (1998) (open pentagons), the gas rich low surface brightness galaxies studied by van Zee et al. (1997) (open squares), and the isolated dIrrs of van Zee, (2000, 2001) (open triangles).